Evaluation of OpenFOAM's discretization schemes used for the convective terms in the context of fire simulations

G. Maragkos[a], S. Verma[b], A. Trouvé[b], B. Merci[a]

[a]Department of Structural Engineering and Building Materials, Ghent University, St. Pietersnieuwstraat 41, B-9000 Ghent, Belgium
[b]Department of Fire Protection Engineering, University of Maryland, College Park, MD 20742, USA

Abstract

The influence of the numerical schemes used for discretization of the convective terms in the momentum equations and in the transport equations for scalars is investigated. To this purpose, a set of problems with exact solutions, the Taylor-Green vortex problem, an isotropic decaying turbulence problem, along with two well-known fire configurations, namely the Sandia's helium plume and McCaffrey's fire plume experiments, are considered for evaluation purposes. Overall, the influence of the employed numerical schemes in both equations is shown to be significant on computational meshes that are typically employed in the context of fire simulations. As expected, the discretization errors diminish when sufficiently fine grid resolutions are considered. The native schemes of OpenFOAM, $filteredLinear2$ and $limitedLinear$, are found to be relatively accurate, when compared to other numerical schemes in the literature: while maintaining boundedness of the solution, they introduce only small amounts of numerical dissipation.

Keywords: numerical schemes, discretization, numerical dissipation, OpenFOAM

Nomenclature

Subscripts

∞ Ambient

max   Maximum

eff	Effective (molecular+turbulent)
f	Face
N	Cell N
NN	Cell downstream of cell N
P	Cell P
PP	Cell upstream of cell P
x, y, z	Directions

Greek symbols

χ	Unit step function (-)
ΔT	Temperature difference (K)
Δt	Time step (s)
λ	Weighting factor (-)
μ	Dynamic viscosity (kg/m/s)
ν	Kinematic viscosity (m^2/s)
ϕ	Scalar (-)
ψ	Flux limiter function (-)
ρ	Density (kg/m^3)

Symbols

$\dot{Q}$	Heat release rate (kW)
A	Surface area (m^2)
A_{EDM}	EDM model parameter (-)
C	Cell center (m)
D	Mass diffusivity (m^2/s)

d Distance (m)

dS Surface area element (m^2)

F Mass flux (kg/s)

f_x Mesh non-uniformity index (-)

k $filteredLinear2$ and $limitedLinear$ scheme parameter (-)

L Length (m)

l $filteredLinear2$ scheme parameter (-)

n Unit vector normal to a surface (-)

p Pressure (Pa)

Q Q-criterion (s^{-2})

t Time (s)

u Velocity (m/s)

V Velocity (m/s) / Volume (m^3)

x, y, z Spatial distances (m)

1. Introduction

Fire safety engineering, nowadays, often relies on the use of Computational Fluid Dynamics (CFD) for numerically simulating a variety of fire scenarios that would be difficult to predict with simplified modelling approaches. The range of fire-related scenarios which are of interest to fire safety engineers can involve multi-scale physics e.g., pollutant dispersion, smoke transport, flame spread and pyrolysis, water spray systems, etc., and a wide range of time/length scales, which typically poses limitations on the levels of grid resolution that can be employed in the simulations. In such cases, often relatively coarse grid sizes have to be employed in order to have numerical predictions within reasonable computational times. In such cases, the numerical schemes used for discretization of the flow equations is likely

to have a significant effect on the final numerical solution in terms of both accuracy and numerical stability.

A pre-requisite for all types of fire-related numerical simulations, either reacting or not, is not only to be stable and to converge to a solution, but to also guarantee boundedness of the solution [1]. For instance, negative values for scalars, e.g., chemical species mass fractions, will very soon render any numerical simulation unstable and is therefore unacceptable. Within this framework, discretization of the convective terms in the transport equations is of great importance, because it is one of the main factors that can lead to unboundedness of the solution [2]. Accurate discretization schemes are, therefore, needed that will not only produce solutions that are free of oscillations, while maintaining the bounds of scalars, but that will also not introduce excessive levels of numerical dissipation. The use of highly diffusive numerical schemes, even though robust, might produce solutions that are not sufficiently accurate and can potentially affect some of the flow characteristics (e.g., puffing frequency of fire plumes and/or air entrainment). On the other hand, higher order numerical schemes, even though more accurate, can be less stable, depending on the scenario at hand. Therefore, a balance between stability, convergence and accuracy is needed when selecting the numerical discretization schemes in numerical simulations.

To date, the OpenFOAM platform [3, 4] has been extensively applied towards simulating a wide range of engineering applications, including fire scenarios (e.g., [5, 6, 7, 8, 9, 10]) with relatively good level of success. Some studies reporting on the influence of the numerical schemes used within the OpenFOAM platform (e.g., [11, 12, 13, 14, 15, 16, 17, 18, 19]), as well as with the use of FireFOAM specifically (e.g., [20, 21, 22, 23]), already exist in the literature, nevertheless their influence when modelling actual fire-related scenarios has not been extensively reported. The main objective of this work is to investigate the accuracy of a selection of native numerical schemes of OpenFOAM, often employed in numerical simulations of fire scenarios. The solver scalarTransportFoam from the OpenFOAM 2.2.x package and Fire-FOAM 2.2.x [24] has been employed in the current study. When applicable, depending on the scenario at hand, a second order implicit backward scheme has been considered for time discretization, a central difference scheme for the diffusive terms, and gradients are evaluated based on a second order least squares method. Focus is on the schemes employed for discretization of the convective terms in the momentum equations and the transport equations for scalars (i.e., chemical species and sensible enthalpy). The paper reports on

4

the accuracy of the selected schemes over a wide range of grid sizes, typical in numerical simulations of fire scenarios. A range of test cases is considered: three problems with exact solutions, the Taylor-Green vortex problem, a decaying isotropic turbulence problem, a non-reacting helium plume case and a set of reacting methane fire plumes. Eventually, the conclusions drawn from this work can provide some guidance to future researchers working on fire modelling with OpenFOAM or FireFOAM with respect to the appropriate selection of numerical discretization schemes in their simulations.

2. Numerical schemes

The use of CFD by definition requires the discretization of the Navier-Stokes equations as well as the transport equations for scalars (i.e., chemical species and sensible enthalpy) [25]. Considering as an example a compressible flow, the momentum equations and transport equation of a passive scalar, ϕ, can be formulated as:

$$\frac{\partial(\rho u)}{\partial t} + \nabla \cdot (\rho u u) = -\nabla p + \nabla \cdot (\mu_{eff} \nabla u) + BF \tag{1}$$

$$\frac{\partial(\rho \phi)}{\partial t} + \nabla \cdot (\rho u \phi) - \nabla(\rho D_\phi \nabla \phi) = 0 \tag{2}$$

where BF denotes any body force present (e.g., gravity).

The focus in this study is on the discretization of the convective terms (i.e., second terms on the l.h.s) of both equations. These terms are discretized using the finite volume method and, employing Gauss' theorem, they can be written as:

$$\int_V \nabla \cdot (\rho u u) dV = \sum_{cell\ faces} F u_f \tag{3}$$

$$\int_V \nabla \cdot (\rho u \phi) dV = \sum_{cell\ faces} F \phi_f \tag{4}$$

where $F = A_f \rho_f u_f$ is the face flux contribution from u while the cell face area is defined as $A_f = \int_f n dS$.

The face values of all variables, defined in Equations (3) and (4), are obtained through interpolations of their cell-centered values. The general equation for calculating the value of a variable, e.g., scalar ϕ, at face f (see Figure 1) reads:

$$\phi_f = \lambda \phi_P + (1 - \lambda)\phi_N \tag{5}$$

with λ a weighting factor which for equidistant meshes is calculated as:

$$\lambda = \frac{1}{2}r + (1-r)\chi \qquad (6)$$

where χ is 1 for outward fluxes from the cell and 0 otherwise, while the parameter r depends on the discretization scheme.
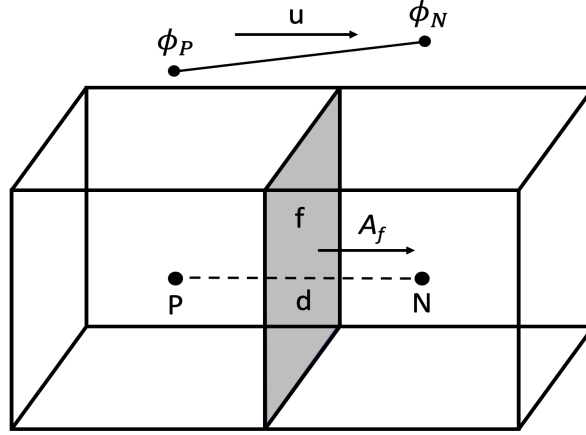

Figure 1: Illustration of two adjacent cells, P and N, with the transport of a scalar ϕ with velocity u. The cell-center distance is d, f denotes the face and A$_f$ is the cell face area.

A brief overview of the different numerical schemes employed for the convection of scalars and vectors from the OpenFOAM platform is presented next.

- Central schemes

  - *linear*: A second order, central difference scheme suitable for isotropic meshes that has limited numerical dissipation. This scheme works as follows:

$$\phi_f = r\phi_P + (1-r)\phi_N \qquad (7)$$

    where $r = fN/PN$, i.e., the ratio of the distance between the center of cell N and the face shared by cells N and P divided by the distance between cells P and N.

- Upwind-biased schemes

6

– *linearUpwind* [25]: A second order, upwind-biased, unbounded scheme (less so than *linear*, though), which employs an explicit correction based on the local cell gradient. The scheme is implemented as:

$$\phi_f = \phi_P + r \cdot (\nabla\phi)_P \tag{8}$$

where r denotes the vector connecting the center of the upwind cell P with the center of the face f (where the value of ϕ is being evaluated) and $(\nabla\phi)_P$ is the gradient of ϕ at the center of the upwind cell P.

– *LUST* [3]: The Linear-Upwind Stabilised Transport scheme is an unbounded fixed blended scheme (25% *linearUpwind* and 75% *linear* weights) that applies an explicit gradient-based correction obtained from the *linearUpwind* scheme. This scheme is implemented as:

$$\phi_f = 0.75(f_x\phi_P + (1 - f_x)\phi_N) + 0.25(\phi_P + r \cdot (\nabla\phi)_P) \tag{9}$$

where f_x represents the mesh non-uniformity in the direction of the vector r (e.g., $f_x = 1/2$ for uniform grids) and the vector r has already been described above.

– *filteredLinear2(V) k l* [3]: A second order, unbounded scheme which attempts to limit the unboundedness of the *linear* scheme. The scheme is implemented as:

$$\phi_f = \begin{cases} (1 - r(1 - f_x))\phi_P + r(1 - f_x)\phi_N & 0 < r < 1 \\ f_x\phi_P + (1 - f_x)\phi_N & 1 \le r \\ \phi_P & \text{elsewhere} \end{cases} \tag{10}$$

where the parameter r is calculated as:

  * $\phi_N - \phi_P > 0$

$$r = (1+l) - k\left(\frac{\min(\max(\Delta\phi - 2d \cdot (\nabla\phi)_P, 0), \max(\Delta\phi - 2d \cdot (\nabla\phi)_N, 0))}{\max(|\Delta\phi|, \max(|2d \cdot (\nabla\phi)_P|, |2d \cdot (\nabla\phi)_N|))}\right) \tag{11}$$

  * $\phi_N - \phi_P \le 0$

$$r = (1+l) - k\left(\frac{\min(\max(2d \cdot (\nabla\phi)_P - \Delta\phi, 0), \max(2d \cdot (\nabla\phi)_N - \Delta\phi, 0))}{\max(|\Delta\phi|, \max(|2d \cdot (\nabla\phi)_P|, |2d \cdot (\nabla\phi)_N|))}\right) \tag{12}$$

7

where $\Delta\phi = \phi_N - \phi_P$, d denotes the vector connecting the center of the upwind cell P with the center of the downwind cell N and $(\nabla\phi)_N$ is the gradient of ϕ at the center of the downwind cell N. The factors k and l are controlled by the user and take values between 0 and 1. This scheme has not been satisfactorily described in the literature, consequently, it is discussed further below.

For uniform grids and 'central difference' approximation of $(\nabla\phi)_P$ and $(\nabla\phi)_N$, r reduces to the following form:

* $\phi_N - \phi_P > 0$

$$r = 1+l-k\left(\frac{\min(\max(\phi_{PP} - \phi_P, 0), \max(\phi_N - \phi_{NN}, 0))}{\max(|\phi_N - \phi_P|, \max(|\phi_N - \phi_{PP}|, |\phi_{NN} - \phi_P|))}\right)$$
(13)

* $\phi_N - \phi_P \leq 0$

$$r = 1+l-k\left(\frac{\min(\max(\phi_P - \phi_{PP}, 0), \max(\phi_{NN} - \phi_N, 0))}{\max(|\phi_N - \phi_P|, \max(|\phi_N - \phi_{PP}|, |\phi_{NN} - \phi_P|))}\right)$$
(14)

Here, PP (NN) represents the cell upstream (downstream) of cell P (N). Equations (13) and (14) suggest the following about this scheme:

* Specifying $k = 0$ reduces this scheme to a *linear* scheme, regardless of the value of the factor l.
* This scheme applies upwinding only if the values of the scalar ϕ at the center of cells PP, P, N and NN form a zigzag pattern, which indicates dispersion issues.
* The factor k scales the amount of overall upwinding that is applied because of the presence of the zigzag pattern; with an increase in k from 0 to 1 leading to higher amount of upwinding, overall.
* As the factor l is increased from 0 to 1 the amount of overall upwinding is reduced independent of the spatial variation of ϕ.

For all cases considered here, the parameter k has been assigned values of either 0.25 or 1, while $l = 0$. The optional keyword V, applicable only to vector fields, denotes that a single limiter is

8

applied to all components of the vector. The limiter is calculated based on the direction of most rapidly changing gradient, resulting in the strongest limiter being applied [3].

- TVD schemes

  The Total Variation Diminishing schemes can generally better capture strong gradients in flows without the spurious oscillations in the solution as created by purely central schemes. The TVD schemes are based on the concept that no new local extrema must be created, while the value of an existing local minimum must be non-decreasing and that of the local maximum must be non-increasing. An overview of the different TVD schemes used in this study is presented below.

  The TVD parameter r is calculated as:

  $$r = 2\frac{d \cdot (\nabla \phi)_P}{\phi_N - \phi_P} - 1 \tag{15}$$

  with the gradient at cell P, $(\nabla \phi)_P$, calculated based on the selected gradient scheme and $d = C_N - C_P$ the distance vector between the centers of the two cells involved.

  Subsequently, ϕ_f can be calculated based on the TVD parameter r as:

  $$\phi_f = \phi_P + \frac{1}{2}\psi(r)(\phi_N - \phi_P) \tag{16}$$

  where $\psi(r)$ is defined below for the schemes considered in this study.

  - *limitedLinear(V) k* [3]: A first/second order, *linear* scheme that limits towards upwind in regions of rapidly changing gradient. The optional keyword V was previously described for $filteredLinear2$. When applied to transport of species mass fractions, the scheme $limitedLinear01$ k is employed, an extension of the scheme specialized for stronger bounding of scalars between 0 and 1.

    $$\psi(r) = \max(\min(2r/k, 1), 0) \tag{17}$$

    with $0 < k \le 1$ a user-input parameter. Parameter $k = 1$ corresponds to strongest limiting (i.e., towards upwind) while this scheme tends towards linear as the coefficient goes to 0. Values

of 0.25, 0.5 and 1 have been considered for k in this study (note that values lower than 0.2 can lead to 'switching' instabilities [23], hence are avoided). It is worth mentioning here that for lower values of k this scheme becomes practically identical to the Gamma scheme [23] by Jasak et al. [31].

– *MUSCL* [26]: The second order Monotonic Upstream-centered Scheme for Conservation Laws.

$$\psi(r) = \max[\min(2r, 0.5(1+r), 2), 0] \qquad (18)$$

– *SuperBee* [27]: A second order scheme (this is the default scheme for LES simulations in the Fire Dynamics Simulator (FDS) code [28]).

$$\psi(r) = \max[\min(2r, 1), \min(r, 2), 0] \qquad (19)$$

The *MUSCL* and *SuperBee* schemes are well described in the literature so they are only briefly described here. An overview of the different TVD limiters considered is presented in Figure 2. The light gray area denotes the TVD region, while the darker gray area denotes the 2nd order TVD region. *Superbee* traverses the upper bound of the second order TVD region while *limitedLinear* 1 traverses the upper bound of the second order TVD region for $r \leq 1$ and the lower bound for $r > 1$. As seen from Figure 2, *limitedLinear* 0.25 - used as an example here - does not behave as a TVD scheme in the region $r < 0.5$. For smooth solutions (i.e., $r \geq 1$) the TVD scheme will tend towards second order accuracy, resulting in accurate flux-conserved convection, while in regions with very sharp gradients (i.e., $r < 1$) it will switch to first order (i.e. upwind) flux-conserved convection.

3. Test cases

Different types of test cases are considered for the evaluation of the accuracy of the different numerical schemes considered in this study. These cases consist of a set of 3 numerical experiments (i.e., exact solutions) for the convection of scalars, 2 test cases for the convection of vectors and finally 2 well-known fire scenarios, in order to evaluate the accuracy of the schemes in practical scenarios.
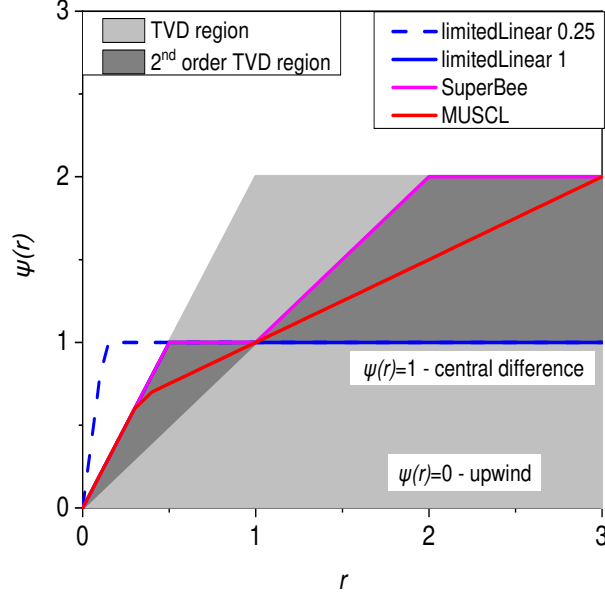
Figure 2: TVD regions [29] for first and second order accurate TVD schemes.

3.1. Numerical experiments

Three test cases involving the convection of a scalar, ϕ, in a square 2D domain of dimensions 1 m × 1 m are considered here. The left and bottom boundaries of the computational domain act as inlets, while the top and right boundaries are outlets. Three structured grid resolutions - 30 × 30, 60 × 60 and 90 × 90 cells - are considered with the mesh-to-flow angle set to 45°. The inlet velocity (m/s) vector at the left and bottom boundaries of the domain is set to (1,1,0). The simulations are run for 100 s, with a maximum Courant-Friedrichs-Lewy (CFL) number of 0.5 (maximum allowed time step of 0.01 s). The numerical schemes considered for these cases are: *limitedLinear k* (with coefficients $k = 0.25, 0.5, 1.0$); *linear*; *MUSCL*; and *SuperBee*. Following [30, 31], three different profiles are set for ϕ at the left inlet boundary (i.e., with x being the vertical direction of the 2D box):

- Step profile:

$$\phi(x) = 1 \quad \text{if } 0 \leq x \leq 1 \tag{20}$$

  corresponding to a case with an abrupt change in the scalar profile (i.e., $\phi(y) = 0$ on the bottom inlet boundary).

11

- $\sin^2$ profile:

$$\phi(x) = \begin{cases} \sin^2[3\pi(x - \frac{1}{6})] & \text{if } \frac{1}{6} \leq x \leq \frac{1}{2} \\ 0 & \text{elsewhere} \end{cases} \tag{21}$$

corresponding to a case with a smoothly changing scalar profile.

- Semi-ellipse profile:

$$\phi(x) = \begin{cases} \sqrt{1 - \left(\frac{x - \frac{1}{3}}{\frac{1}{6}}\right)^2} & \text{if } \frac{1}{6} \leq x \leq \frac{1}{2} \\ 0 & \text{elsewhere} \end{cases} \tag{22}$$

corresponding to a case with an abrupt change in the scalar profile on the edges of the semi-ellipse, followed by a smooth scalar change over the elliptic part.

Comparisons of the simulated profiles on a line parallel to the left inlet (i.e. $y = 0.333$ m) are presented for the $\sin^2$ and semi-ellipse profile cases, while they are shown on a diagonal line (i.e., from top left to bottom right corner given by equation $x + y = 1$) for the step profile case.

Results from the simulations of the 3 test cases with different numerical schemes, as a function of grid size, are presented in Figures 3-5. As expected, the differences between the numerical schemes diminish with increasing grid resolution, essentially resulting in similar predictions on the finest grid size (i.e., 90×90 cells). Nevertheless, some interesting observations can be made regarding the performance of each numerical scheme. The coefficient k in the *limitedLinear* scheme has a significant influence in the predictions on the coarsest grid size employed. Lowering the coefficient to values below 1, effectively introducing some central discretization in the scheme, improves the predictions, while still maintaining boundedness of the solution. Clear oscillations in the solutions are present with the *linear* scheme, with values not staying bounded between 0 and 1. Overall, the predictions of both $MUSCL$ and *limitedLinear* 1 are comparable, but they are the most dissipative of the numerical schemes tested. The predictions of *limitedLinear* 0.25 and $SuperBee$ are also comparable. However, the *limitedLinear* 0.25 is slightly more dissipative in the $\sin^2$ profile case, while the $SuperBee$ does not perform well in the semi-ellipse case: it transforms the solution into a top-hat

profile for the 60×60 and 90×90 cell test cases. Nevertheless, $SuperBee$ performs quite accurately on the coarsest grid size (30×30 cells) case considered here. The $limitedLinear$ 0.5 scheme is, overall, slightly more dissipative than $limitedLinear$ 0.25. If coarse grid sizes are to be employed in numerical simulations of fire scenarios and use of the $limitedLinear$ k is to be made, then it is preferable to assign the parameter values of $k \approx 0.25 - 0.5$ in order to avoid the excessive numerical dissipation introduced by the scheme.

A comparison between the predictions with the various numerical schemes for the coarse grid (i.e., 30×30 cells) and fine grid (i.e., 90×90 cells) cases, previously presented in Figures 3-5, is given in Table 1. Focus has been given on several aspects including accuracy of the solution, boundedness of the scalar between 0 and 1 as well as on the introduced numerical dissipation in the solution (i.e., predicted scalar value compared to the analytical solution). The comparison presented in Table 1 mainly aims to serve as a quick reference guide of the performance of the numerical schemes in the different test cases.

Table 1: Comparison of the different numerical schemes used in the simulations. Comparison symbols: ++ (very accurate), + (accurate), - (not accurate), - - (least accurate).
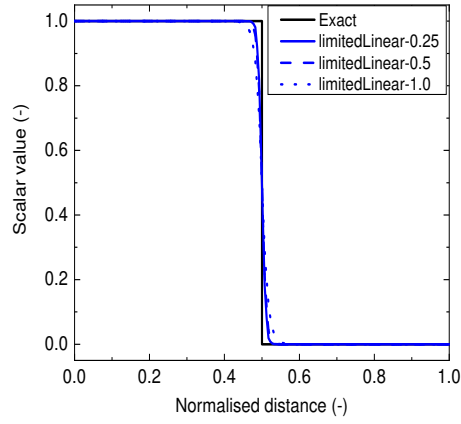
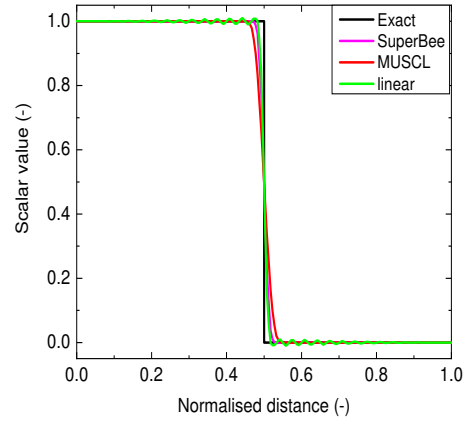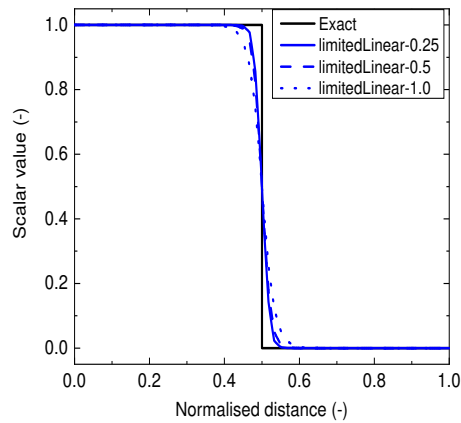|	step profile	$\sin^2$ profile	semi-ellipse profile
Coarse grid: 30×30 cells			
$limitedLinear$ 0.25	++	++	+
$limitedLinear$ 0.5	++	+	+
$limitedLinear$ 1.0	+	-	-
$SuperBee$	++	++	++
$MUSCL$	+	-	-
$linear$	-	- -	- -
Fine grid: 90×90 cells			
$limitedLinear$ 0.25	++	++	++
$limitedLinear$ 0.5	++	++	++
$limitedLinear$ 1.0	+	+	+
$SuperBee$	++	++	-
$MUSCL$	+	+	+
$linear$	- -	+	- -

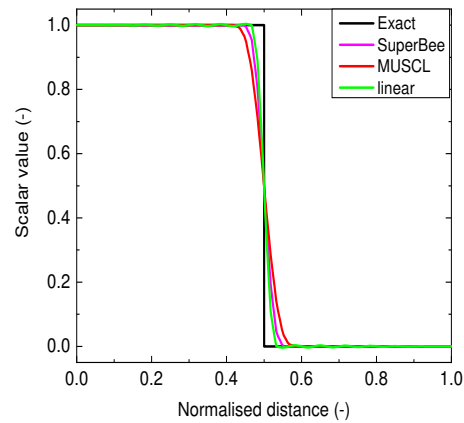(a) 90×90 cells
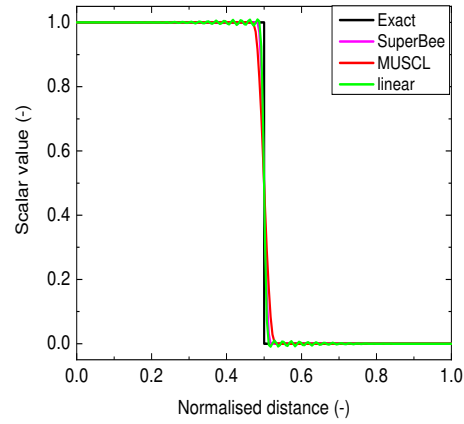
(b) 90×90 cells
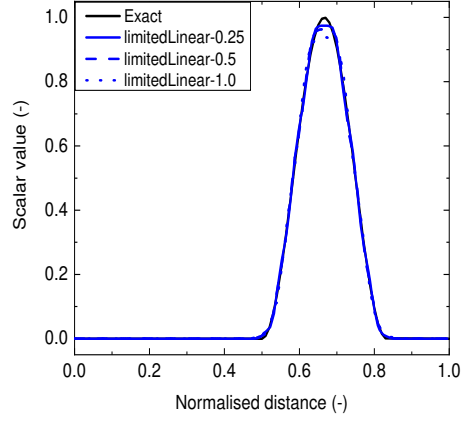
(c) 60×60 cells
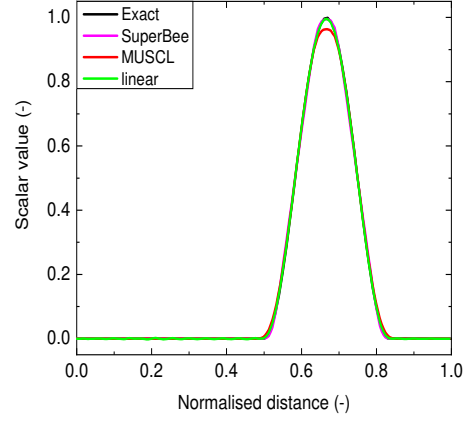
(d) 60×60 cells

(e) 30×30 cells

(f) 30×30 cells

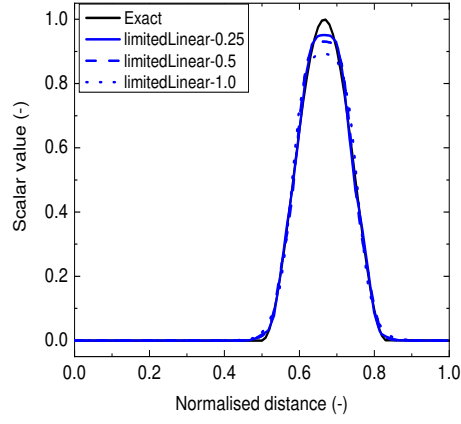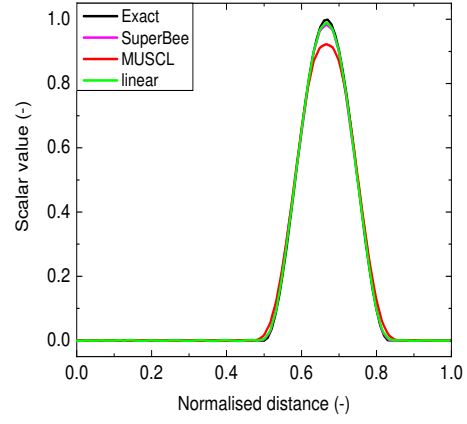Figure 3: Convection of a step profile, 45°, with different schemes.

14
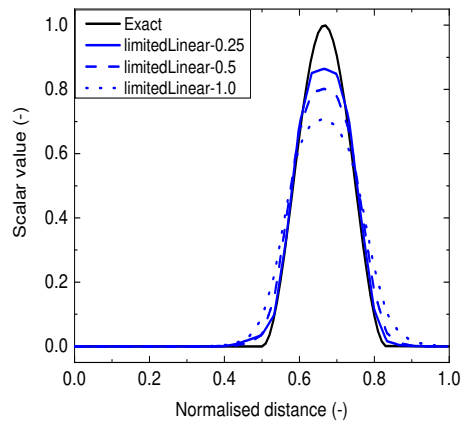
(a) 90×90 cells

(b) 90×90 cells

(c) 60×60 cells

(d) 60×60 cells

(e) 30×30 cells

(f) 30×30 cells

Figure 4: Convection of a $\sin^2$ profile, 45°, with different schemes.
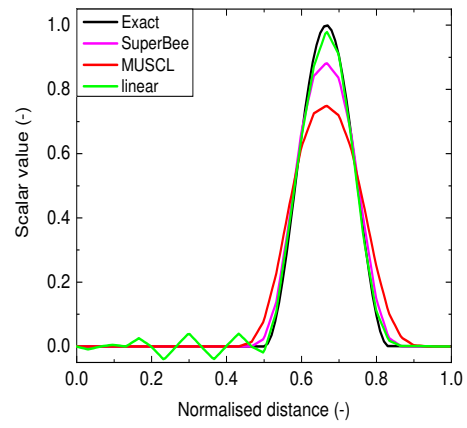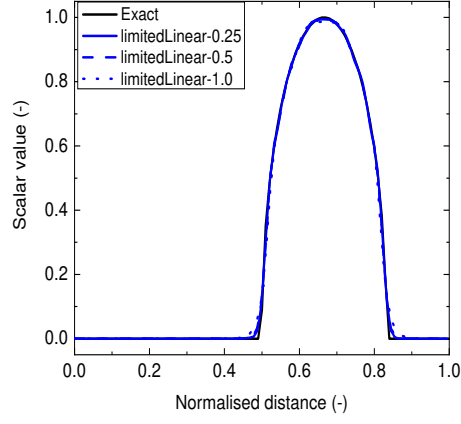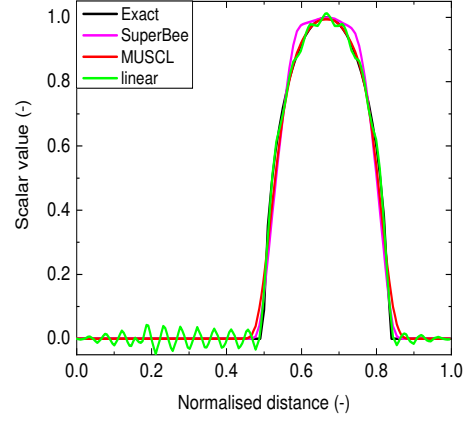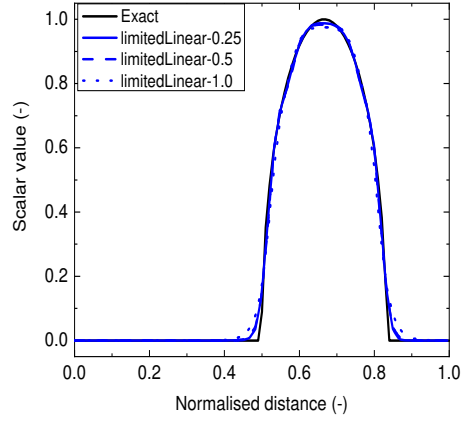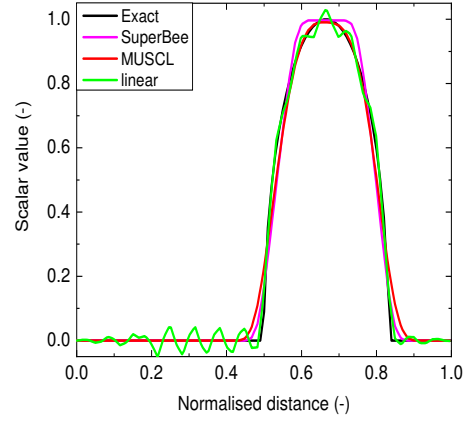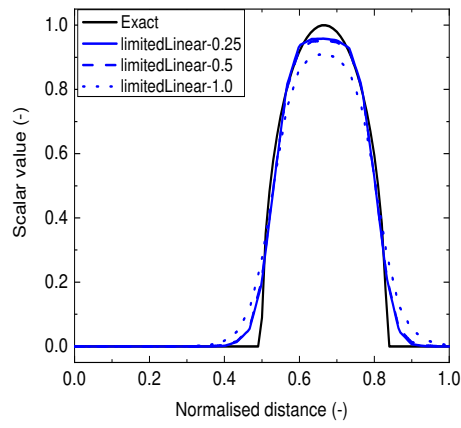
(a) 90×90 cells
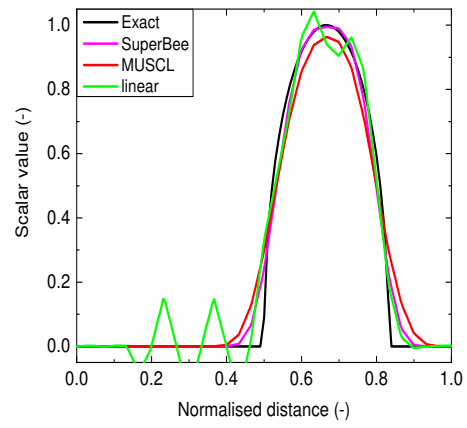
(b) 90×90 cells

(c) 60×60 cells

(d) 60×60 cells

(e) 30×30 cells

(f) 30×30 cells

Figure 5: Convection of a semi-ellipse profile, 45°, with different schemes.

3.2. Taylor-Green vortex

The next case considered is the classical Taylor-Green vortex problem
[36], a three-dimensional unsteady inviscid flow of a decaying vortex in which
the turbulent energy cascade can be studied numerically. The case involves
well-defined initial and boundary conditions, making it a suitable benchmark
test case for CFD validation. The initial analytical solution contains a single
length scale, but due to the non-linear interactions of the developing eddies
this results in a fully turbulent dissipative spectrum. Numerical simulations
of this problem can be used for the evaluation of the dissipation and conser-
vation properties of the numerical schemes employed, hence, the temporal
evolution of the enstrophy (defined as half the square of the magnitude of
the vorticity vector) and kinetic energy is of interest. Given the inviscid
nature of the flow in this case ($\nu = 0$), the kinetic energy in the numerical
simulations should remain constant, equal to its initial value, while the en-
strophy will grow rapidly. Any decrease in the turbulent kinetic energy will
be due to numerical dissipation introduced by the discretization schemes.
Comparisons will be made to the semi-analytical solution for the enstrophy
growth by Brachet et al. [37]. A periodic box of dimensions $(2 \times \pi)^3$ m^3 and
three different sets of grid resolutions (32^3, 64^3, 128^3) are employed in the
simulations. The simulations are run for 10 s, with a maximum CFL number
of 0.5 (maximum allowed time step of 0.01 s). The initial conditions [41] for
density, velocity and pressure in the Taylor–Green vortex case read:

$$\rho = 1 \qquad (23)$$

$$u = \begin{cases} u_x = \sin(x)\cos(y)\cos(z) \\ u_y = -\cos(x)\sin(y)\cos(z) \\ u_z = 0 \end{cases} \qquad (24)$$

$$p = p_\infty + \frac{1}{16}[\cos(2x) + \cos(2y)][2 + \cos(2z)] \qquad (25)$$

where p_∞ is the ambient pressure and the temperature is initialised using the
ideal gas law.

The numerical simulation results, overall, reproduce to a great extent
what has been reported in literature in the past regarding the Taylor-Green
vortex problem. The initial large vortices start to eventually break down
while still maintaining their global structure ($t < 3$ s) until they eventually
start to become unstable around $t \geq 4$ s [37], progressively generating smaller

17

structures (i.e., resulting in an increase of enstrophy) [40]. This is illustrated in Figure 6 where, following the work of [21], the instantaneous snapshots of the iso-surface $Q = 0.15$ s^{-2} (Q is the second invariant of the velocity gradient tensor) colored by the velocity magnitude with $filteredLinear2V$ 1 for the 128^3 case are presented.

(a) $t = 0$ s
(b) $t = 2.5$ s

(c) $t = 5$ s
(d) $t = 10$ s
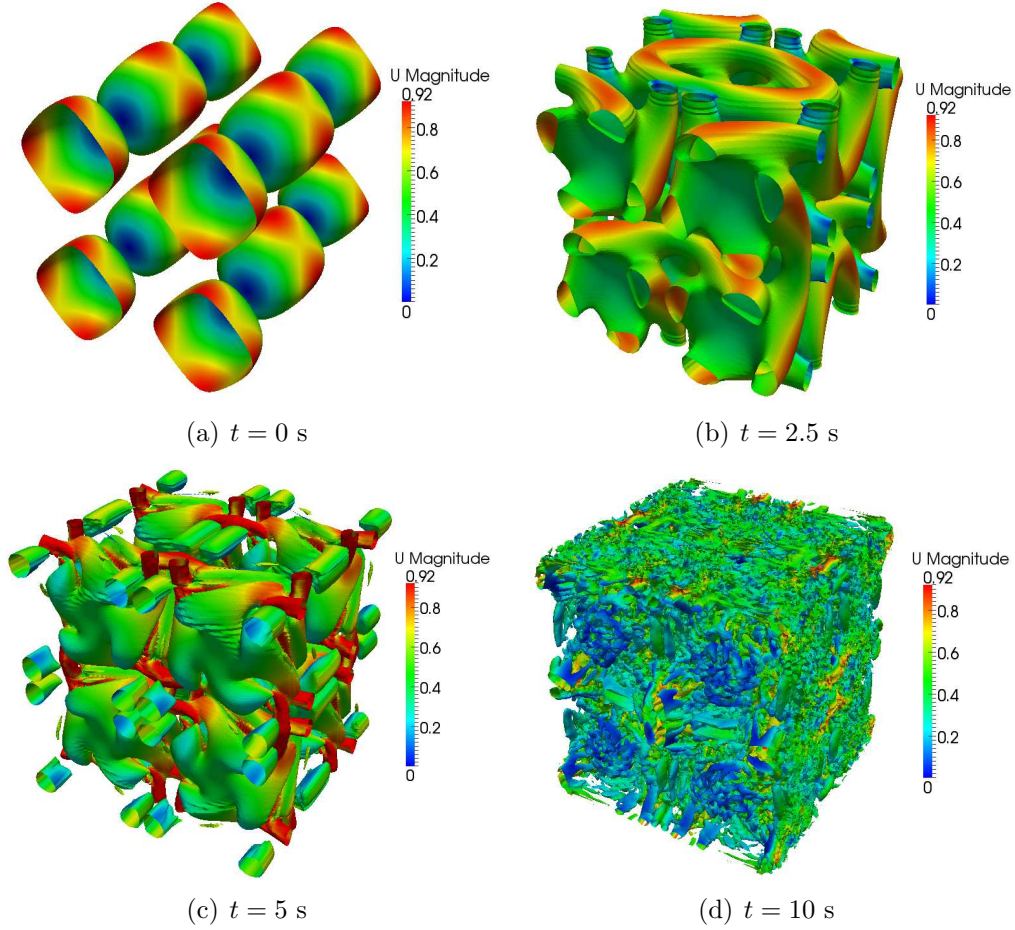
Figure 6: Instantaneous snapshots of the iso-surface $Q = 0.15$ s^{-2} colored by the velocity magnitude with $filteredLinear2V$ 1 for the 128^3 case.

The conservation properties of the numerical schemes can be evaluated by examining the time during which the kinetic energy remains constant. Examining the time evolution of the enstrophy also provides information regarding the dissipation introduced by the schemes. Results of both quantities, nor-

malized by their initial values, for different schemes as a function of grid size are presented in Figures 7 and 8 while a more quantitative comparison is given in Table 2.

Figure 7: Time history of normalized (a) kinetic energy and (b) enstrophy as a function of grid resolution with $filteredLinear2V$ 1 and $linear$.

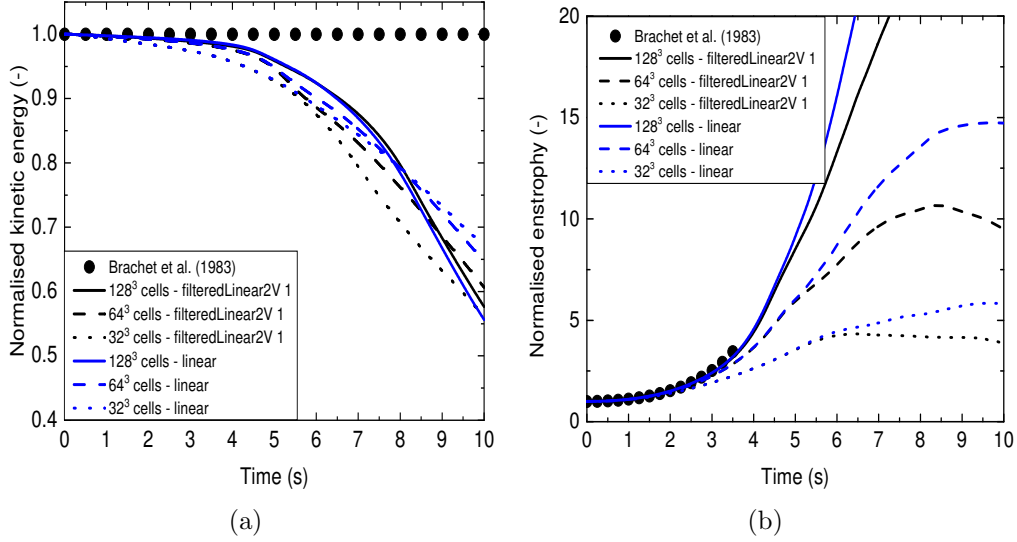A rapid decrease for the turbulent kinetic energy is observed with all schemes for the 32^3 cases, given the coarseness of the mesh, followed by a small increase in the enstrophy. Increasing the grid resolution helps preserving the turbulent kinetic energy for longer periods of time, with the best predictions obtained for the 128^3 grid size. In this case, a sudden increase in the enstrophy is predicted starting from $t > 4$ s for all schemes, with notably higher values obtained with the $filteredLinear2V$ 1 and $linear$ schemes. According to Brachet et al. [37], a singularity exists in the inviscid limit around $t \approx 5.2$ s, meaning that the normalized enstrophy would tend to infinity. This is not truly encountered in the present simulations, given the levels of grid resolution employed and the artificial dissipation added by the numerical schemes. It is expected that significant improvements in the predictions would be obtained from the use of higher order numerical schemes and finer grid resolutions. From the predicted values of turbulent kinetic energy and enstrophy, presented in Table 2, it is obvious that some numerical dissipation is present in the numerical simulations, particularly for the 64^3 case. In this case, the $filteredLinear2V$ 1 scheme was slightly more dissipative

Table 2: Comparison of the normalized kinetic energy and enstrophy (64^3 and 128^3 cases) for the Taylor-Green vortex, with the semi-analytical solution of Brachet et al. [37].

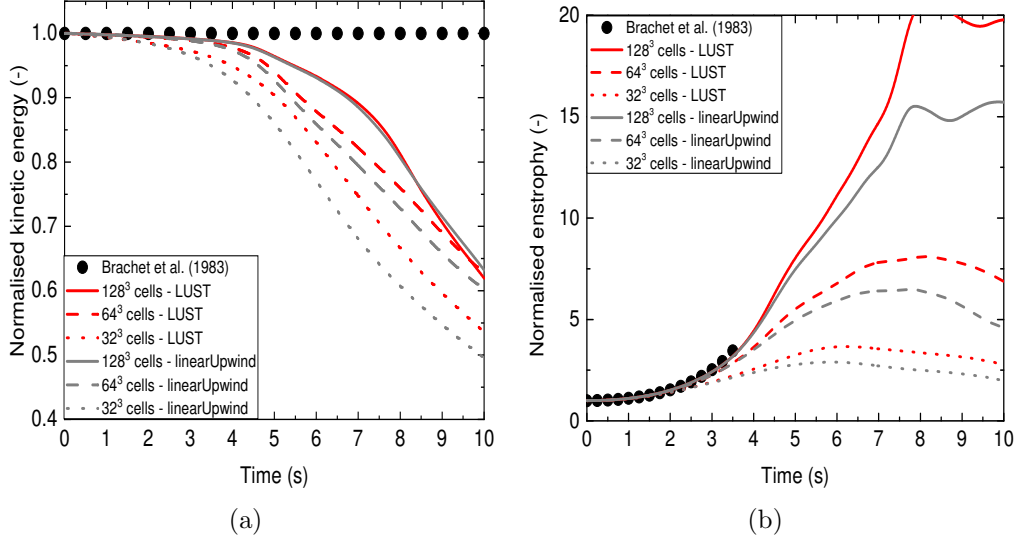|	Normalized kinetic energy ($t = 5$ s)	Normalized enstrophy ($t = 3.5$ s)
Brachet et al. [37]	1	3.457
Johnsen et al. [41] (64^3 case)	1	3.33
64^3 case		
$linear$	0.948	2.850
$filteredLinear2V$ 0.25	0.947	2.846
$filteredLinear2V$ 1	0.946	2.843
$limitedLinearV$ 0.25	0.928	2.825
$limitedLinearV$ 1	0.914	2.808
$linearUpwind$	0.927	2.827
$LUST$	0.940	2.855
128^3 case		
$linear$	0.961	3.210
$filteredLinear2V$ 0.25	0.960	3.176
$filteredLinear2V$ 1	0.959	3.163
$limitedLinearV$ 0.25	0.952	3.142
$limitedLinearV$ 1	0.948	3.137
$linearUpwind$	0.963	3.183
$LUST$	0.964	3.192

Figure 8: Time history of normalized (a) kinetic energy and (b) enstrophy as a function of grid resolution with $LUST$ and $linearUpwind$.

than the $linear$ scheme. Nevertheless, the $filteredLinear2V$ 1 has improved boundedness properties compared to $linear$, which can be important for numerical stability. Higher order numerical schemes would be needed for spatial discretization in order to reduce the numerical dissipation [41], including a higher order scheme for time discretization. If this is not possible, then increasing the grid resolution, combined with small CFL numbers, can help remedy these problems to some extent.

Following the work of Abdelsamie et al. [38], comparisons are also made to the 2-D Taylor-Green vortex case which is well documented in the literature (e.g., [39]), involving an incompressible flow with constant density and viscosity, and for which an analytical solution exists. A periodic square box of side $L = 2 \times \pi$ m is used, the grid resolution is set to 64^2, 128^2 and 256^2, the kinematic viscosity is equal to $\nu = 1.26 \times 10^{-4}$ m^2/s while the numerical simulations are set to run for 10 s with a time step of $\Delta t = 5 \times 10^{-4}$s [38]. Comparisons between the numerical simulations and the analytical solution of the 2-D Taylor-Green vortex problem are presented in Table 3 for selected numerical schemes. The performance of the various numerical schemes is reasonable for all cases examined with the maximum relative deviations remaining between 0.45% (for $linearUpwind$) – 0.75% (for $linear$ / $filteredLinear2V$) for the 64^2 grid resolution and decrease to 0.02% (for

21

linearUpwind) - 0.04% (for *linear / filteredLinear2V*) for the 256^2 grid resolution. Not surprisingly, the predictions are less satisfactory when compared to the results reported in Abdelsamie et al. [38] where high-fidelity codes were employed and the maximum relative deviations for a 64^2 grid resolution remained below 1.3×10^{-3}%. The numerical results reported here do suggest that lower-order methods can achieve an accuracy close to the one of higher-order methods but with a higher grid resolution. In addition, the profiles of the two velocity components along both centerlines of the domain are compared to the analytical solution in Figure 9. Overall, the profiles predicted by the simulations (Figure 9) are visually in very good agreement with the analytical solution.

Table 3: Comparison of the maximum velocity and the relative deviation at $t = 10$ s as a function of grid size for the 2-D Taylor–Green vortex case.

	Maximum velocity (m/s)	Relative deviation (%)
Analytical	0.9875778	Reference
64^2 case		
linear	0.9801318	0.75
filteredLinear2V 1	0.9801318	0.75
linearUpwind	0.9831560	0.45
LUST	0.9815091	0.61
128^2 case		
linear	0.9853916	0.22
filteredLinear2V 1	0.9853916	0.22
linearUpwind	0.9866962	0.09
LUST	0.9862037	0.14
256^2 case		
linear	0.9871434	0.04
filteredLinear2V 1	0.9871434	0.04
linearUpwind	0.9874093	0.02
LUST	0.9873157	0.03

3.3. Decaying isotropic turbulence

The case considered here is the low Reynolds number experiment of Comte-Bellot and Corrsin (CBC) [32], consisting of an unforced flow, so that
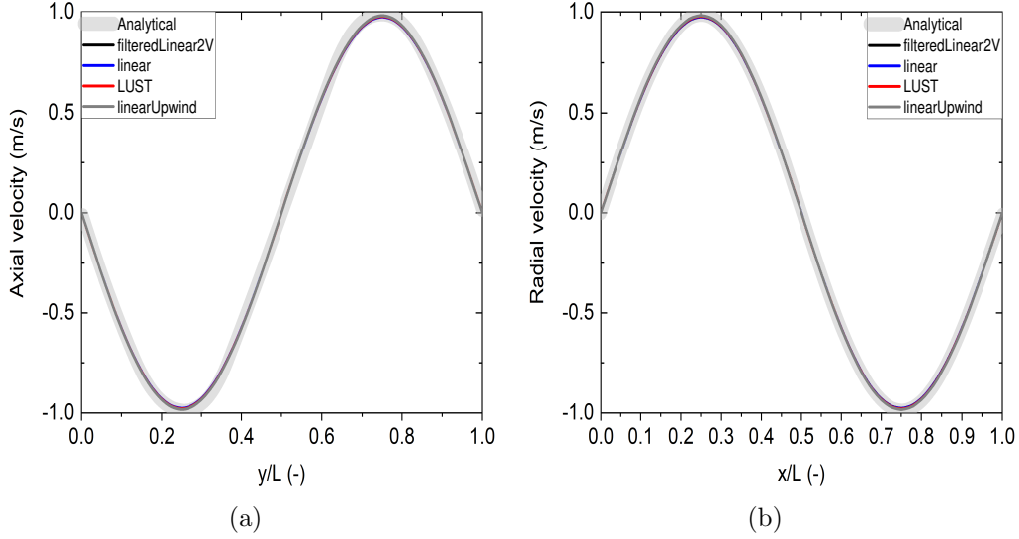
Figure 9: Comparison of the (a) axial and (b) radial velocity along both centerlines of the domain for different schemes with the analytical solution for the 2-D Taylor–Green vortex at $t = 10$ s with a grid resolution of 64^2. The setup of the numerical simulations is based on Abdelsamie et al. [38].

the decay of the total kinetic energy in time is due to viscous dissipation. A periodic box of side $L = 0.18 \times \pi (\approx 0.566$ m$)$ with grid resolutions of 32^3 and 64^3 is considered. The kinematic viscosity is set to $\nu = 1.5 \times 10^{-5}$ m^2/s while turbulence is modelled with the dynamic Smagorinsky model. The resolved component of the turbulent kinetic energy was approximated as 0.0642 m^2/s^2 (i.e. for the 64^3 case obtained after applying a low-pass filter to the CBC energy spectrum) while the unresolved sub-grid scale component is equal to 0.0135 m^2/s^2 (i.e., distributed homogeneously across the computational domain) [21]. The simulations are run for 1 s, with a maximum CFL number of 0.5 (maximum allowed time step of 0.01 s). The initial condition for the simulation was generated by superimposing Fourier modes with random phases such that the spectrum matched that of the initial experimental data [33], and is taken from [34]. An illustration of the initial and final states of the velocity magnitude for the 64^3 case is presented in Figure 10.

Comparisons are made to experimental measurements of the resolved turbulent kinetic energy at three specific times, equal to 0, 0.28 and 0.66 s. Figure 11 presents a comparison between the numerical simulations with the different numerical schemes employed in the simulations and the CBC data.
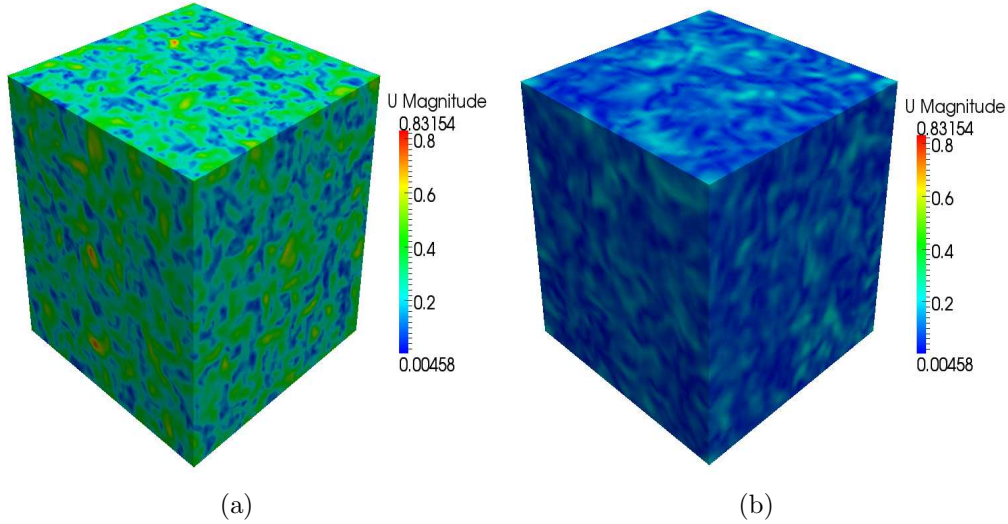
Figure 10: Illustration of the (a) initial ($t = 0$ s) and (b) final ($t = 1$ s) velocity magnitudes with $filteredLinear2V$ 1 in the 64^3 case.

A more quantitative comparison of the predicted turbulent kinetic energies with the different numerical schemes is presented in Table 4. The numerical predictions with $linear$, $filteredLinear2V$ 0.25 and $filteredLinear2V$ 1 are, overall, comparable and close to the experiments for both grid resolutions tested, with some small discrepancies present in the 64^3 case (i.e., under-prediction of the turbulent kinetic energy). Following these schemes, $LUST$ is slightly more dissipative, but still captures the decrease of the turbulent kinetic energy fairly well. The application of either the $limitedLinearV$ 0.25, $limitedLinearV$ 1 or $linearUpwind$ results in increased amounts of numerical dissipation, as noted from the faster decrease of the turbulent kinetic energy. These findings further strengthen the conclusions drawn from the Taylor-Green vortex problem, namely that $filteredLinear2V$ is a relatively low-dissipation numerical scheme, when compared to $linear$, and is thus suitable for the discretization of the convective term in the momentum equations. For completeness, and because it is relevant for the comparison presented here, it is reported that the resulting domain-averaged Smagorinsky constant (not shown here) was of the order of 0.15-0.16, which is slightly lower than the theoretical value of 0.16-0.17 [35].
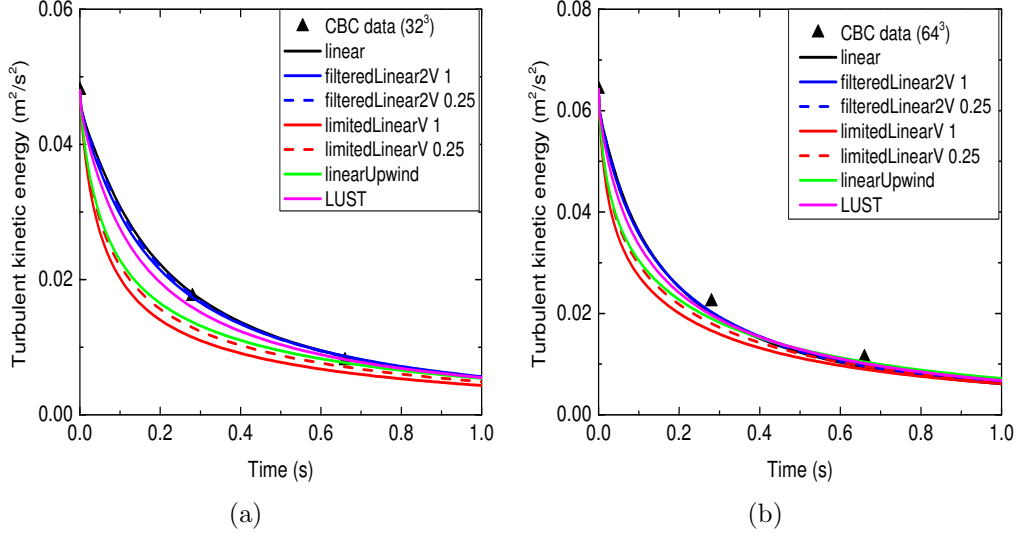
24

Figure 11: Time history of resolved turbulent kinetic energy for a grid resolution of (a) 32^3 and (b) 64^3 with different numerical schemes.

Table 4: Comparison of the predicted turbulent kinetic energy with different numerical schemes against the experimental data of Comte-Bellot and Corrsin (CBC) [32].

	Kinetic energy (m^2/s^2) $t = 0.28$ s	Kinetic energy (m^2/s^2) $t = 0.66$ s
	32^3 case / 64^3 case	32^3 case / 64^3 case
CBC data [32]	0.0175 / 0.0223	0.0080 / 0.0113
$linear$	0.0178 / 0.0201	0.0086 / 0.0094
$filteredLinear2V$ 1	0.0173 / 0.0203	0.0087 / 0.0098
$filteredLinear2V$ 0.25	0.0176 / 0.0201	0.0086 / 0.0096
$limitedLinearV$ 1	0.0114 / 0.0166	0.0062 / 0.0090
$limitedLinearV$ 0.25	0.0128 / 0.0180	0.0071 / 0.0095
$linearUpwind$	0.0137 / 0.0189	0.0077 / 0.0104
$LUST$	0.0159 / 0.0196	0.0081 / 0.0101

25

3.4. Helium plume

Comparisons are made with Sandia's helium plume experiments as reported by O'Hern et al. [42]. The plume source is 1 m in diameter, surrounded by a 0.5 m wide floor, issued from a diffuser at an average velocity of 0.325 m/s. The mixture at the source contains 96.4% helium (He), 1.7% acetone (C_3H_6O) and 1.9% oxygen (O_2) by volume, with a molecular weight of 5.45 g/mol. The reported experimental uncertainty on the measured helium mass fractions are in the order of 23%. A cylindrical computational domain of 4 m × 4 m is employed to model the case and a grid sensitivity study is considered. The base mesh consists of approximately 6 cm cells employing a local grid refinement strategy which further refines the grid size in the near-field region just above the helium plume source. A first cylinder of dimensions 2 m × 2 m refines the mesh to 3 cm while a second cylinder of dimensions 1.5 m × 1 m refines the mesh to 1.5 cm. Following the experiments, the reported mixture composition is applied at the inlet. The ambient temperature and pressure are set to 285 K and 80900 Pa, respectively. Turbulence is modelled with the dynamic Smagorinsky model with a variable turbulent Schmidt number formulation. The simulations are run for 35 s, based on a maximum CFL number of 0.9, with averaging over the last 30 s to produce mean values. These settings have proven to be accurate in the past for this test case [43].

Figures 12-13 present the radial profiles of the predicted (axial / radial) velocities and helium mass fractions at two different heights (i.e., $y = 0.2$ m and $y = 0.6$ m) above the plume inlet as a function of grid size. Focus is given on analyzing the influence of the numerical schemes used for discretization of the convective terms in the momentum and species mass fraction equations.

Overall, differences between the various schemes used for the convective term in the momentum equations are mainly observed for the predicted axial velocities (Figure 12(a)). Apart from the results on the coarsest grid size (i.e., 6 cm), all other numerical predictions are within the experimental uncertainty with $filteredLinear2V$ 1 and $linear$ being close and slightly higher than the experimental data and $LUST$ slightly under-predicting the experimental values. Overall, a stronger grid sensitivity is observed with $LUST$, when examining the results with 6 cm and 3 cm / 1.5 cm grids, compared to the other two schemes employed. Additionally, the predictions with $filteredLinear2V$ 1 are typically close to the ones of $linear$. The differences in the predicted radial velocities remain small between the different schemes (Figure 12(b)).

Figure 13 presents the predicted helium mass fractions with different schemes used for the convective term in the species equations and with $filteredLinear2V$ 1 used for the convective term in the momentum equation. Overall, the predictions with $limitedLinear$ 0.25 are closest to the experimental values at both axial locations and for all different grid sizes examined. The differences between the schemes at height $y = 0.6$ m (Figure 13(b)) remain small, with all simulations over-estimating the helium mass fractions. The discretization errors diminish with reduced grid cell size. Hence, it is no surprise that the predictions with the different schemes are similar for the finest grid size (i.e., 1.5 cm). Nevertheless, the influence of the numerical schemes on the coarsest grid (i.e., 6 cm) is non-negligible. The $limitedLinear$ 1 scheme is found to be more dissipative than the other two (i.e., $limitedLinear$ 0.25 and $SuperBee$) for grid sizes of 3 cm and 6 cm, due to the limiting towards upwind in this scheme. Based on these results, lowering the coefficient k in the $limitedLinear$ scheme is suggested when coarse grids are used, in order to reduce the numerical dissipation.

The over-predictions reported for the helium mass fractions in Figure 13(b) could be attributed to several reasons. More specifically, there are uncertainties regarding the experimental inlet boundary conditions (i.e., honeycomb structure and turbulence level at the inlet), whether consideration of the whole experimental facility when modelling the case is essential, what exactly is being reported as mass fractions from the experiments (i.e., whether it is pure helium or whether it contains acetone as well) and any errors in the experimental measurements themselves. These are well-known issues when it comes to this test case and are part of ongoing research in the community. In addition, there can also be potential deficiencies related to turbulence modelling (i.e., not accounting for back-scatter as well as the accuracy of the turbulence model itself), diffusion modelling (i.e., need for a more advanced diffusion model than Fick's law or more accurate calculation of the species' mass diffusivities) or actually some influence of the considered numerical schemes in the simulations (e.g., higher order and/or more accurate schemes might still be required).

The discretization scheme used for convection in the momentum equation (i.e., $filteredLinear2V$ 1 vs $linear$) did not have a significant influence on the resulting (axial / radial) velocities for all grid sizes employed in the simulations (Figure 12). On the other hand, some small differences were observed with the use of $LUST$. Figure 14, presenting 2-D plots of the velocity magnitudes in the near-field region just above the helium plume source for
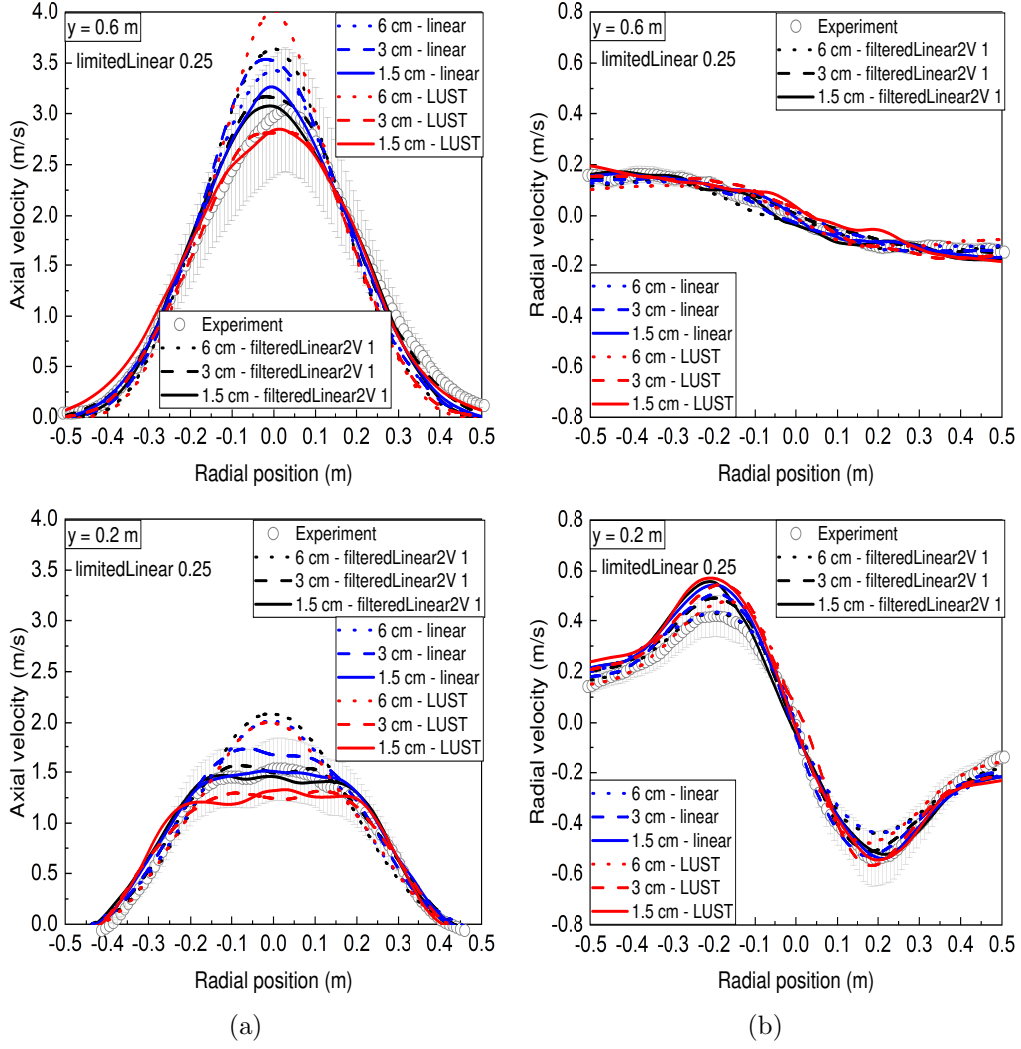
27

Figure 12: Radial profiles of (a) axial velocity and (b) radial velocity at heights $y = 0.2$ m and $y = 0.6$ m with *limitedLinear* 0.25 for species mass fraction and different schemes for velocity.
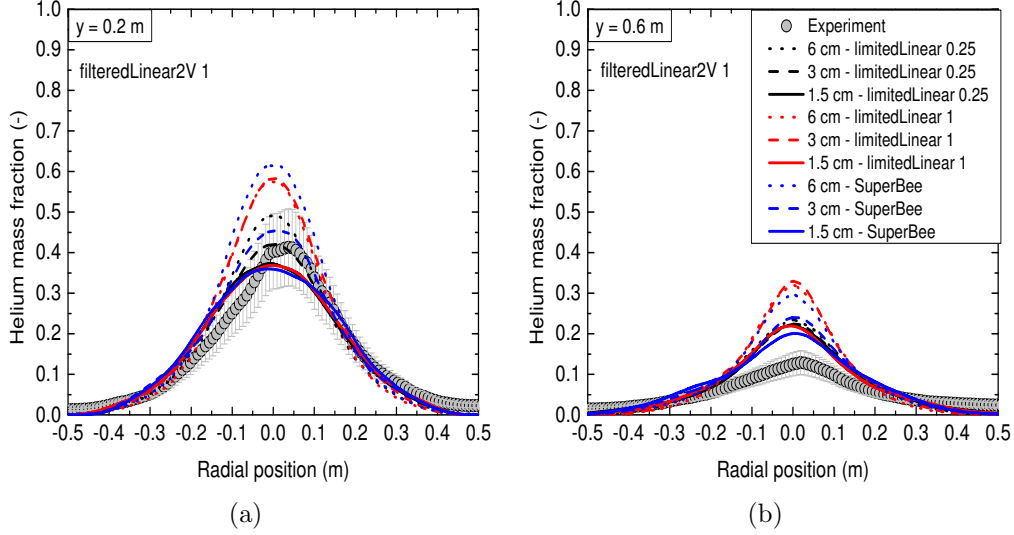
Figure 13: Radial profiles of helium mass fractions at height (a) $y = 0.2$ m and (b) $y = 0.6$ m with $filteredLinear2V$ 1 for velocity and different schemes for species mass fractions. The legend is identical for both subfigures.

the finest grid size (i.e., 1.5 cm) with the three different schemes, further supports this statement. The predictions with $filteredLinear2V$ 1 appear to be slightly more dissipative when compared to $linear$, but the overall flow field is not significantly different. However, lower velocities are qualitatively obtained with $LUST$ when compared to either $linear$ or $filteredLinear2V$ 1.

3.5. Methane fire plumes

McCaffrey's experiments [44] consist of a 30 cm square burner using natural gas as fuel. The burner is raised 75 cm from the ground and the heat release rates are 14.4 kW, 21.7 kW, 33 kW, 44.9 kW and 57.5 kW. The interesting feature of these experiments is that the experimental data of centerline temperature and velocity collapse when scaled by the Froude number. A rectangular computational domain of 3 m × 3.3 m × 3 m is employed in this case with the burner raised 30 cm from the bottom boundary. The base mesh consists of 6 cm cells employing a local mesh refinement strategy in order to have good grid resolution up to the experimentally reported flame height. A first box of dimensions 1.5 m × 3.3 m × 1.5 m refines the mesh to 3 cm while a second box of dimensions 0.9 m × 1.8 m × 0.9 m refines the mesh to 1.5 cm. The fuel in the numerical simulations is considered to be methane.
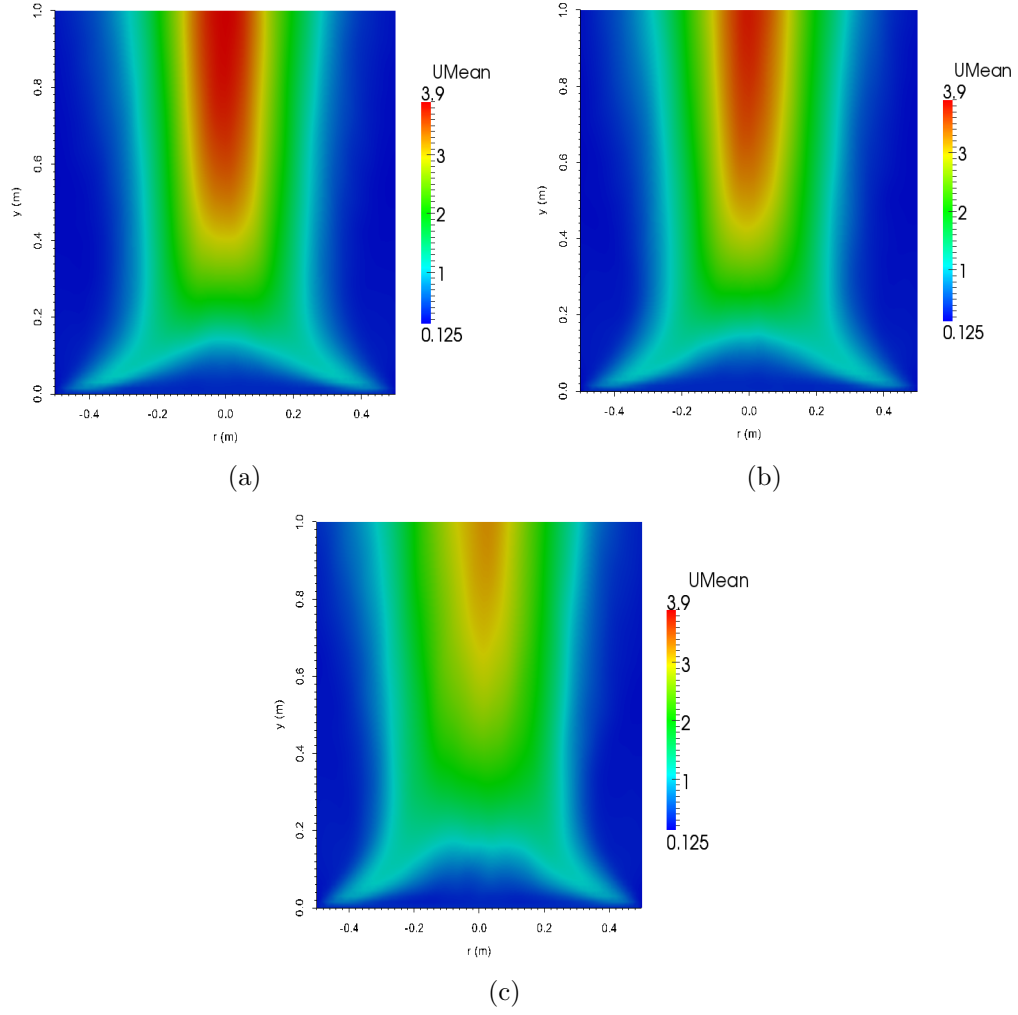
(a)

(b)

(c)

Figure 14: 2-D plots of velocity magnitude with (a) *linear*, (b) *filteredLinear2V* 1 and (c) *LUST* for a grid size of 1.5 cm.

The ambient temperature and pressure are set to 293 K and 101325 Pa, respectively. Turbulence is modelled with the dynamic Smagorinsky model employing a variable turbulent Prandtl number formulation. Combustion is modelled with the Eddy Dissipation Model (EDM) assigning a model constant of $A_{EDM} = 2$ [45]. Radiation is modelled with the finite volume implementation of the Discrete Ordinate Method (fvDOM), assuming an optically thin medium, with the emission term based on the (global) radiative fraction approach (prescribed a-priori based on the experimental measurements). In total, 72 solid angles were used for angular discretization in the solution of the radiative transfer equation (i.e., with radiation solved every 20th time step). The simulations are run for 35 s, with a maximum CFL number of 0.9, averaging over the last 30 s to produce mean results. These settings have proven to be accurate in the past for this test case [43].

The predictions of the mean centerline temperatures and axial velocities with $linear$, $filteredLinear2V\ 1$ and $LUST$ used for the discretization of the momentum equations, along with $limitedLinear$ 0.25 used for the discretization of the transport equations of the scalars (i.e., chemical species and sensible enthalpy), are presented in Figure 15. Overall, both the absolute values and the predicted (temperature / velocity) scaling are satisfactory when $filteredLinear2V\ 1$ is employed with the predictions following McCaffrey's correlations. The predictions with $linear$ show significantly higher temperatures in the flame region and there is more scatter, for both the temperatures and velocities, in the intermittent region. The predictions with $LUST$ are, overall, less satisfactory compared to all the other cases particularly when examining the temperature/velocity scaling in the intermittent region. A more quantitative comparison between the numerical predictions with the different schemes and the experimental data is reported in Table 5. It is worth noting that differences in results due to the choice of numerical scheme for a given (sub-grid scale) turbulence model can potentially be comparable to differences due to the (sub-grid scale) turbulence model for a given numerical scheme, on a fixed mesh. In Table 4 the comparisons, of the results from the present study, to both the experimental data of McCaffrey [44] and results reported by Maragkos et al. [43] reveal that the influence of the numerical schemes can indeed be important and on the same order of magnitude as the influence of the turbulence model (i.e., affecting both the absolute values and the temperature / velocity scaling). Overall, even with grid resolutions on the order of cm, which are typically considered (more than) sufficient for fire plume modelling, the influence of the numerical schemes can still be

(a) *linear*   (b) *linear*

(a) *filteredLinear2V 1*   (b) *filteredLinear2V 1*
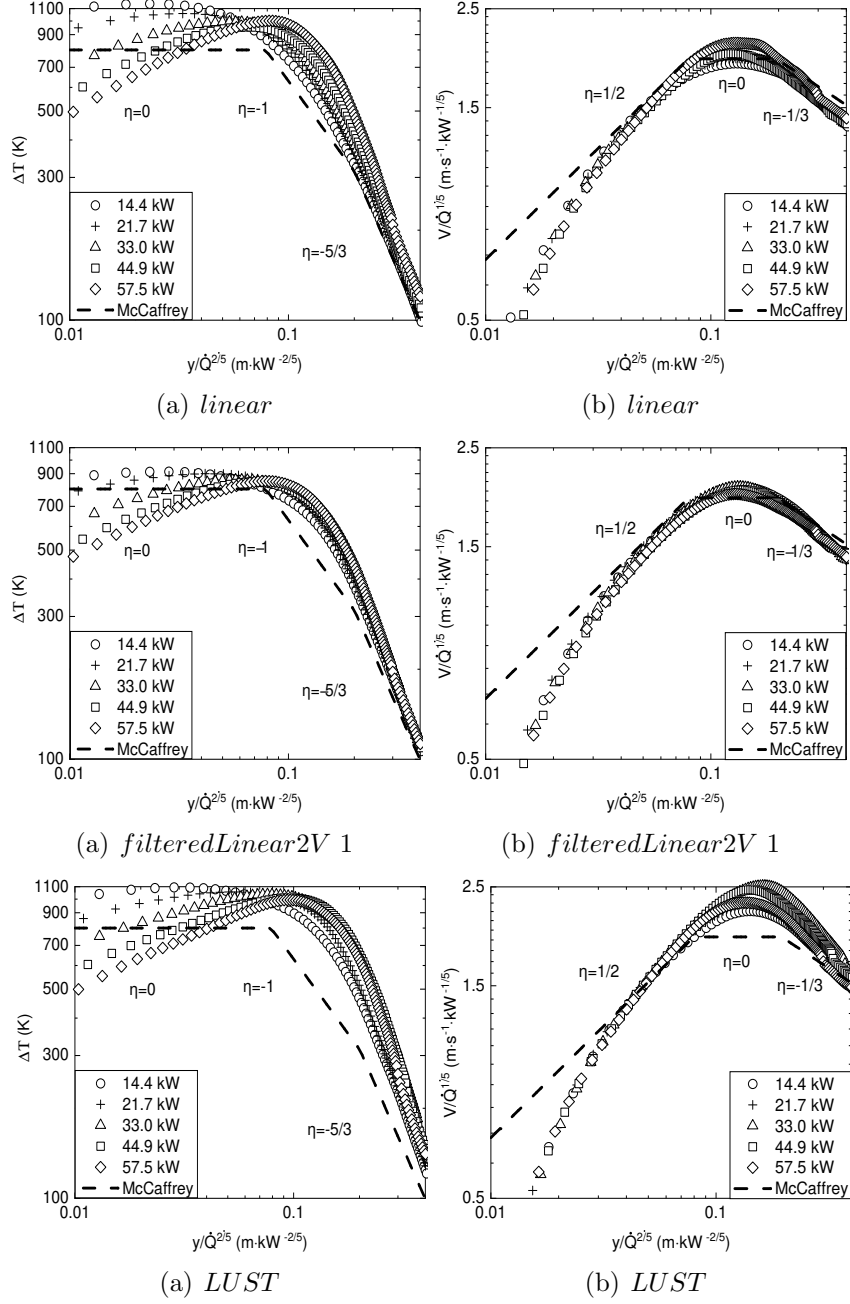

(a) *LUST*   (b) *LUST*

Figure 15: Centerline mean (a) temperatures and (b) axial velocities with different schemes for velocity and *limitedLinear* 0.25 for scalars.

important and requires attention when simulating such scenarios. However, it is worth noting that the solution of a numerical simulation will also be strongly dependent on other modelling aspects e.g., combustion, radiation and soot modelling. The results presented here aim to raise awareness to the OpenFOAM users who conduct fire-related simulations that a careful choice of discretization schemes (i.e., schemes that introduce low numerical dissipation) can be an important aspect in the simulations alongside the other modelling choices.

Table 5: Comparison of the current predictions against the numerical results of Maragkos et al. [43] and the experimental results by McCaffrey [44]. DS: Dynamic Smagorinsky model, CS: Constant Smagorinsky model with $c_s = 0.17$. Comparison symbols: ++ (very accurate), + (accurate), - (not accurate), - - (least accurate).

Case	ΔT or V scaling	Flame region ΔT_{max} (K)	Intermittent region $(V/\dot{Q}^{1/5})_{max}$ (m s^{-1}kW$^{-1/5}$)
Experimental correlation [44]	Yes	800	1.93
linear and DS	+	1142 (43%)	1.92-2.1 (0-9%)
*filteredLinear*2V 1 and DS	++	914 (14%)	1.95-2.05 (1-6%)
LUST and DS	-	1094 (37%)	2.2-2.5 (14-30%)
*filteredLinear*2V 1 and CS [43]	-	803 (0.5%)	2.3-2.55 (19-32%)

4. Conclusions

A comprehensive study was performed, focusing on evaluating some of the native numerical schemes of OpenFOAM [3] for the discretization of the convective terms in the momentum equations and transport equations of scalars: $filteredLinear2$ and $limitedLinear$, respectively. The test cases used for validation purposes involved a set of problems with exact solutions [31], the Taylor-Green vortex problem [36], an isotropic decaying turbulence problem [32], Sandia's helium plume experiments [42] and the fire plume experiments by McCaffrey [44].

The main conclusions of the present study are as follows:

- When it comes to scalar transport, the $limitedLinear$ k scheme was shown to reproduce quite accurately the three different exact solutions (i.e., step profile, sin^2 profile and semi-ellipse profile) considered if the

coefficient k (i.e., blending central difference and upwind schemes) was changed from 1 to values $k \approx 0.25 - 0.5$, still maintaining boundedness of the solution and not exhibiting any oscillations. Overall, the predictions with $limitedLinear$ were comparable to/better than the results obtained with other well-known schemes in literature. The application of the scheme in the helium plume case confirmed these findings with the numerical predictions exhibiting little grid dependency and agreeing very well with the experimental data. The numerical predictions from the application of the scheme in the McCaffrey's fire plume cases were also satisfactory.

- The predictions from the discretization of the convective term in the momentum equations with the $filteredLinear2$ scheme performed satisfactorily in all the test cases considered. Overall, the scheme exhibited small amounts of numerical dissipation when compared to pure central differencing (i.e., $linear$ scheme). Both the predicted enstrophy growth in the Taylor-Green vortex problem and the decay of the turbulent kinetic energy in the case of the isotropic decaying turbulence scenario were reasonably well predicted with this scheme. No significant differences were observed in the helium plume case between the $filteredLinear2$ and $linear$ schemes, however the predictions of $filteredLinear2$ were superior compared to other schemes (i.e., $linear$ and $LUST$) in the McCaffrey's fire plume cases. The choice of the coefficient k in the $filteredLinear2$ scheme (e.g., $k = 0.25$ or $k = 1$) had a small effect in the numerical predictions for the test cases considered, with $k = 1$ being slightly more dissipative than $k = 0.25$.

- The influence from the numerical schemes was, as expected, closely linked to the grid resolution in the numerical simulations. Improved predictions in terms of decaying turbulent kinetic energy, enstrophy growth or kinetic energy conservation in inviscid flows can be achieved by employing higher order numerical schemes for spatial discretization and/or time discretization, as well as using smaller cell sizes and smaller time steps (i.e., lower CFL number). Finally, the numerical simulations of the inviscid Taylor-Green vortex problem revealed that there is a need for better kinetic energy preserving schemes. This aspect will ensure that any influence / errors from the discretization schemes on the numerical predictions will be diminished, particularly on coarse

grids.

Acknowledgments

References

[1] N.P. Waterson, H. Deconinck, Design principles for bounded higher-order convection schemes – a unified approach, J. Comput. Phys. 224 (2007) 182-207. https://doi.org/10.1016/j.jcp.2007.01.021

[2] J.H. Ferziger, M. Peric, Computational Methods for Fluid Dynamics, Springer, 1999.

[3] www.openfoam.com

[4] H.G. Weller, G. Tabor, H. Jasak, C. Fureby, A tensorial approach to computational continuum mechanics using object-oriented techniques, Comput. Phys. 12 (1998) 620-631. https://doi.org/10.1063/1.168744

[5] N. Ren, Y. Wang, S. Vilfayeau, A. Trouvé, Large eddy simulation of turbulent vertical wall fires supplied with gaseous fuel through porous burners, Combust. Flame 169 (2016) 194-208. https://doi.org/10.1016/j.combustflame.2015.12.008

[6] G. Maragkos, T. Beji, B. Merci, Advances in modelling in CFD simulations of turbulent gaseous pool fires, Combust. Flame 181 (2017) 22-38. https://doi.org/10.1016/j.combustflame.2017.03.012

[7] G. Maragkos, B. Merci, Large eddy simulations of CH_4 fire plumes, Flow Turb. Combust. 99 (2017) 239-278. https://doi.org/10.1007/s10494-017-9803-4

[8] G. Maragkos, T. Beji, B. Merci, Towards predictive simulations of gaseous pool fires, Proc. Combust. Inst. 37 (2019) 3927-3934. https://doi.org/10.1016/j.proci.2018.05.162

[9] V.M. Le, A. Marchand, S. Verma, R. Xu, J. White, A.W. Marshall, T. Rogaume, F. Richard, J. Luche, A. Trouvé, Simulations of a turbulent line fire with a steady flamelet combustion model coupled with models for non-local and local gas radiation effects, Fire Safety J. 106 (2018) 105-113. https://doi.org/10.1016/j.firesaf.2019.04.011

[10] I. Sikic, S. Dembele, J. Wen, Non-grey radiative heat transfer modelling in LES-CFD simulated methanol pool fires, J. Quant. Spectrosc. Radiat. Transf. 234 (2019) 78-89. https://doi.org/10.1016/j.jqsrt.2019.06.004

[11] E. Robertson, V. Choudhury, S. Bhushan, D.K.Walters, Validation of OpenFOAM numerical methods and turbulence models for incompressible bluff body flows, Comput. Fluids 123 (2015) 122-145. https://doi.org/10.1016/j.compfluid.2015.09.010

[12] S.B. Lee, A study on temporal accuracy of OpenFOAM, Int. J. Nav. Arch. Ocean. 9 (2017) 429-438. https://doi.org/10.1016/j.ijnaoe.2016.11.007

[13] F.P. Kärrholm, F. Tao, On Performance of Advection Schemes in the Prediction of Diesel Spray and Fuel Vapour Distributions, 22nd European Conference on Liquid Atomization and Spray Systems, 8-10 September 2008, Como Lake, Italy.

[14] Y. Cao, T. Tamura, Large-eddy simulations of flow past a square cylinder using structured and unstructured grids, Computers & Fluids 137 (2016) 36-54. https://doi.org/10.1016/j.compfluid.2016.07.013.

[15] T. Mukha, S. Rezaeiravesh, M. Liefvendahl, A library for wall-modelled large-eddy simulation based on OpenFOAM technology, Comput. Phys. Commun. 239 (2019) 204-224. https://doi.org/10.1016/j.cpc.2019.01.016

[16] C. Greenshields, H. Weller, L. Gasparini, J. Reese, Implementation of semi-discrete, non-staggered central schemes in a colocated, polyhedral, finite volume framework, for high-speed viscous flows, Int. J. Numer. Methods Fluids 63 (2010)1-21. https://doi.org/10.1002/fld.2069

[17] V. Vuorinen, J. Keskinen, C. Duwig, B. Boersma, On the implementation of low-dissipative Runge–Kutta projection methods for time depen-

dent flows using OpenFOAM, Computers & Fluids 93 (2014) 153-163. https://doi.org/10.1016/j.compfluid.2014.01.026

[18] S. Deshpande, L. Anumolu, M. Trujillo, Evaluating the performance of the two-phase flow solver interfoam, Comput. Sci. Discov. 5 (2012) 014016. https://doi.org/10.1088/1749-4699/5/1/014016

[19] J. Martínez, F. Piscaglia, A. Montorfano, A. Onorati, S. Aithal, Influence of spatial discretization schemes on accuracy of explicit LES: Canonical problems to engine-like geometries, Computers & Fluids 117 (2015) 62-78. https://doi.org/10.1016/j.compfluid.2015.05.007

[20] S. Vilfayeau, Large Eddy Simulation of Fire Extinction Phenomena, PhD thesis, University of Maryland, 2015. https://doi.org/10.13016/M2QB0M

[21] S. Vargas-Córdoba, Assessment of the FireFoam model and development of a user's guide, Master thesis, University of Maryland, 2018.

[22] W. Shiyun, Verification tests of mass conservation for FireFOAM and development of a user's guide, Master thesis, University of Maryland, 2019. https://doi.org/10.13016/hepp-rqy6

[23] S. Verma, A large eddy simulation study of the effects of wind and slope on the structure of a turbulent line fire, PhD thesis, University of Maryland, 2019. https://doi.org/10.13016/zya3-indx

[24] https://github.com/fireFoam-dev

[25] F. Moukalled, L. Mangani, M. Darwish, The Finite Volume Method in Computational Fluid Dynamics: An advanced introduction with Open-FOAM and MATLAB, Springer, 2016.

[26] B. Van Leer, Towards the ultimate conservative difference scheme III, Upstream-centered finite-difference schemes for ideal compressible flow, J. Comput. Phys. 23 (1977) 263-275. https://doi.org/10.1016/0021-9991(77)90094-8

[27] P.L. Roe, Characteristic-based schemes for the Euler equations, Annu. Rev. Fluid Mech. 18 (1986) 337-365. 10.1146/annurev.fl.18.010186.002005

[28] Fire Dynamics Simulator (FDS) available through https://pages.nist.gov/fds-smv/

[29] P.K. Sweby, High Resolution Schemes Using Flux Limiters for Hyperbolic Conservation Laws, SIAM J. Numer. Anal. 21 (1984) 995-1011. https://doi.org/10.1137/0721062

[30] B.P. Leonard, The ULTIMATE conservative difference scheme applied to unsteady one-dimensional advection, Comp. Methods Appl. Mech. Eng. 88 (1991) 17-74. https://doi.org/10.1016/0045-7825(91)90232-U

[31] H. Jasak, H.G. Weller, A.D. Gosman, High resolution NVD differencing scheme for arbitrarily unstructured meshes, Int. J. Numer. Meth. Fluids 31 (1999) 431-449. https://doi.org/10.1002/(SICI)1097-0363(19990930)31:2¡431::AID-FLD884¿3.0.CO;2-T

[32] G. Comte-Bellot, S. Corrsin, Simple Eulerian time correlation of full-and narrow-band velocity signals in grid-generated, 'isotropic' turbulence, J. Fluid Mech., 48 (1971) 273-337. https://doi.org/10.1017/S0022112071001599

[33] K. McGrattan, S. Hostikka, R. McDermott, J. Floyd, M. Vanella, Fire Dynamics Simulator Technical Reference Guide Volume 2: Verification, NIST Special Publication 1018-2, Sixth Edition, 2018.

[34] https://github.com/firemodels/fds/tree/master/Verification/Turbulence

[35] S.B. Pope, Turbulent Flows, Cambridge University Press, 2000.

[36] G. Taylor, A. Green, Mechanism of the production of small eddies from large ones, Proceedings of the Royal Society of London A: Mathematical, Physical and Engineering Sciences 158 (1937) 499-521. https://doi.org/10.1098/rspa.1937.0036

[37] M.E. Brachet, D.I. Meiron, S.A. Orszag, B.G. Nickel, R.H. Morf, U. Frisch, Small-scale structure of the Taylor–Green vortex, J. Fluid Mech. 130 (1983) 411-452. https://doi.org/10.1017/S0022112083001159

[38] A. Abdelsamie, G. Lartigue, C.E. Frouzakis, D. Thévenin, The Taylor–Green vortex as a benchmark for high-fidelity combustion simulations using low-Mach solvers, Computers & Fluids 223 (2021) 104935. https://doi.org/10.1016/j.compfluid.2021.104935.

[39] A. Abdelsamie, G. Fru, T. Oster, F. Dietzsch, G. Janiga, D. Thévenin, Towards direct numerical simulations of low-Mach number turbulent reacting and two-phase flows using immersed boundaries, Comput. Fluids, 131 (2016) 123-141. http://dx.doi.org/10.1016/j.compfluid.2016.03.017

[40] J. B. Chapelier, M. De La Llave Plata, F. Renac, Inviscid and viscous simulations of the Taylor-Green vortex flow using a modal discontinuous Galerkin approach, in 42nd AIAA Fluid Dynamics Conference and Exhibit, pp. 2012-3073, 2012.

[41] E. Johnsen, J. Larsson, A.V. Bhagatwala, W.H. Cabot, P. Moin, B.J. Olson, P.S. Rawat, S.K. Shankar, B. Sjögreen, H.C. Yee, X. Zhong, S.K. Lele, Assessment of high-resolution methods for numerical simulations of compressible turbulence with shock waves, Journal of Computational Physics 229 (2010) 1213-1237. https://doi.org/10.1016/j.jcp.2009.10.028

[42] T.J. O'Hern, E.J. Weckman, A.L. Gerhart, S.R. Tieszen, R.W. Schefer, Experimental study of a turbulent buoyant helium plume, J. Fluid Mech. 544 (2005) 143-171. https://doi.org/10.1017/S0022112005006567

[43] G. Maragkos, B. Merci, On the use of dynamic turbulence modelling in fire applications, Combust. Flame 26 (2020) 9-23. https://doi.org/10.1016/j.combustflame.2020.02.012

[44] B.J. McCaffrey, Purely Buoyant Diffusion Flames: Some Experimental Results, National Bureau of Standards, NBSIR 79-1910, 1979.

[45] E.A. Brizuela, R.W. Bilger, On the eddy break-up coefficient, Combust. Flame 104 (1996) 208-212. https://doi.org/10.1016/0010-2180(95)00205-7